Experiments in Fluids (2006) 41: 479–486
DOI 10.1007/s00348-006-0175-0

RESEARCH ARTICLE

Y. Sung · W. Kim · M. G. Mungal · M. A. Cappelli

Aerodynamic modification of flow over bluff objects by plasma actuation

Received: 22 December 2005 / Revised: 29 May 2006 / Accepted: 31 May 2006 / Published online: 18 July 2006

Abstract Particle image velocimetry and smoke visualization are used to study the alteration of the flow field in the wake of a bluff body by use of an alternating current (AC) surface dielectric barrier discharge. Staggered, surface, and buried electrodes were positioned on the downstream side of circular cylinders at conditions of $Re_D = 1 \times 10^4 - 4 \times 10^4$ configured to impose a force due to the ion drift that is either along or counter to the free-stream flow direction. Smoke visualization and Particle Image Velocimetry (PIV) in the wake of the flow confirms that the configuration of the surface electrodes and operation of the discharge significantly alters the location of the flow separation point and the time-averaged velocity profiles in the near and distant wake. Measurements of the vibrational and the rotational temperature using optical emission spectroscopy on the N_2 second positive system ($C^3\Pi_u$–$B^3\Pi_g$) indicates that the resulting plasma is highly non-equilibrium and discounts the possibility of a thermal effect on the flow separation process. The mechanism responsible for reduction or enhancement of flow separation is attributed to the streamwise force generated by the asymmetric ion wind—the direction of which is established by the electrode geometry and the local surface charge accumulated on AC cycles.

1 Introduction

The aerodynamic drag on bluff bodies is determined mainly by the inability of the flow pressure to recover on the downstream side due to flow separation (wake formation). Flow separation is caused by the presence of an adverse pressure gradient in the vicinity of the surface, acting upon the boundary layer fluid, which has slowed owing to the action of friction. Separation leads to a shear layer that becomes unstable, forming large-scale vortices and an unsteady wake. Flow separation can be delayed or overcome altogether by methods such as appropriately streamlining the body, surface blowing, surface suction or base bleed. Blowing imparts streamwise momentum to the surface-adjacent fluid to assist in overcoming the adverse pressure field.

Recently, it has been found that surface direct-current (DC) corona and alternating (AC) dielectric-barrier discharges (DBDs) also seem to stabilize boundary layers where separation may otherwise occur (Roth et al. 2000; Artana et al. 2002, 2003; Roth 2003; Enloe et al. 2004a, b; Post and Corke 2004). In either of the DC or AC discharge configurations, the discharge generates a plasma in the immediate vicinity of the surface of the aerodynamic body. In the case of an AC DBD, the ions of this plasma drift in response to the time-varying electric field, a component of which is parallel to the surface. The presence of a dielectric causes an unequal plasma density and therefore, ion drag in the two swings of the AC cycle with the ionic wind velocity "following" the AC high voltage frequency (Forte et al. 2005). The result is a larger volumetric ion momentum transfer to the neutral fluid during the phase of the cycle when the accumulated electron charge on the dielectric surface streams back toward the positively-biased top electrode, as shown through particle-in-cell simulations (Font 2004). If the electrodes (which are often simply metallic strips between a dielectric sheet) are configured such that the net force due to the ion drift is along the streamwise direction, then flow separation can be suppressed, as illustrated in our findings below. Conversely, electrodes can also be configured to induce separation, generating an unusually large wake, as also demonstrated below. Such a configuration, while undesirable from an aerodynamic standpoint, may be suitable in applications requiring enhanced flow mixing.

Y. Sung · W. Kim · M. G. Mungal (✉) · M. A. Cappelli
Mechanical Engineering Department,
Stanford University, Stanford, CA 94305, USA
E-mail: mungal@stanford.edu
Tel.: +1-650-7231745
Fax: +1-650-7231748

The use of gas discharge phenomena to alter atmospheric aerodynamic flows is not a new concept (Malik et al. 1983). The use of corona discharges to produce and accelerate ions via the generation of an ion wind and to alter the thickness of aerodynamic boundary layers has been well studied (El-Khabiry and Colver 1997; Artana et al. 2002, 2003; Hyun and Chun 2003). It was found that the ion wind generated by these corona discharges reduced drag by as much as 50% in flows with Reynolds number of $\sim 10^5$ (El-Khabiry and Colver 1997). However, the discharge configuration was difficult to scale and integrate into practical devices. With the exception of the very high voltage DC corona operating condition referred to as the "generalized glow regime" (Artana et al. 2002, 2003), high pressure dielectric barrier discharges seem to better conform to large surface areas (Roth and Sherman 1998; Roth et al. 2000) and have been used in applications extending beyond the control of aerodynamic flows, such as in the optical pumping of CO_2 lasers, large-area mercury-free fluorescent lamps, flat plasma display panels, and ozone generation (Kogelschatz et al. 1997). In principle, dielectric barrier discharges can generate diffuse uniform coverage, depending on the gas used, ambient pressure, electrode separation, operating voltage, and operating AC frequency as has been shown through the parametric studies of Pons et al. (2005). However, in practice, the plasmas generated in air are often filamentary and made up of individual electron avalanche discharges. For the aerodynamic flow control described here, the discharges were filamentary (i.e., three-dimensional on the scale of the electrode separation) in form.

2 Experimental set-up

The dielectric barrier discharge flow actuator was of an asymmetric design similar to that used by Roth and Sherman (1998), and simulated by Font (2004). A schematic of the general features of the discharge is shown in Fig. 1. The actuator is made up of a flow-exposed copper-tape electrode (0.1 mm thick, 2 mm wide) that extends transverse to the flow and a similar offset electrode covered by a thin (0.3 mm) dielectric polycarbonate sheet. Such a sheet plasma electrode-pair actuator (or multiple pairs of actuators) can be easily mounted onto the surface of an aerodynamic body such as a cylinder, which is the bluff body studied here. When an alternating high voltage is applied across the electrodes, a gas discharge plasma is sustained by the resulting alternating current (AC) between the exposed electrode and the dielectric surface just above the covered electrode. Polycarbonate was chosen as the dielectric material in this study due to its high melting point, its availability in various thicknesses, and its ability to easily conform to aerodynamic surfaces. The operating frequency for the studies described here is 40 kHz and the applied voltage was varied systematically to understand its effect on the ability of the discharge to influence the flow. The voltage was applied across the electrodes using a Dynage, Model 860–308 power supply and was monitored using a high voltage probe (North Star Research Corp., NM, USA, PVM-10). The buried electrode was at variable high potential, while the electrode exposed to the flow was at ground potential. The discharge current was monitored by measuring the voltage across a 50 Ω shunt resistor using a passive voltage probe with a 10X attenuation (Tektronix, OR, USA, P6109B).

An example of a discharge formed in air using an actuator sheet containing two electrode-pair strips is shown in the photograph to the left in Fig. 2. The configuration for this particular discharge is schematically illustrated to the right of this photograph. Although the plasma appears diffuse and uniform, it is actually made up of microscale filaments, as verified by the discharge current traces (described below) for the frequencies used here.

The configuration of an electrode pair on the sheet actuator can be such that the ion wind imparts a streamwise force on the flow at some point on the cylinder surface, as illustrated schematically in Fig. 3a. Also studied is the reverse configuration, with the exposed electrode placed downstream of the buried electrode, to impart a net force against the flow (see Fig. 3b). As shown in the schematics of Fig. 3, electrode pairs were positioned at various locations in the downstream portion of the cylinder cross section for the smoke-visualization studies (discussed below).

Smoke visualization of the altered flowfield due to plasma actuation was carried out in a 10×100 cm smoke visualization tunnel capable of generating air velocities in excess of 5 m/s. Six electrode pairs were placed on the surface of a 10 cm diameter cylinder symmetrically about the symmetry plane at angles of $\pm$ 90, 120, and 150° from the forward stagnation

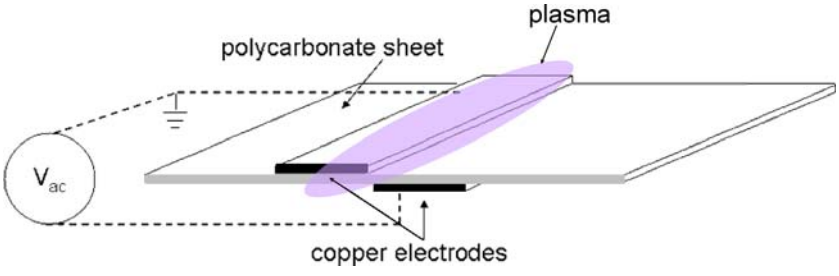

Fig. 1 Illustrative schematic of a typical dielectric barrier discharge excited by a single pair of staggered strip electrodes

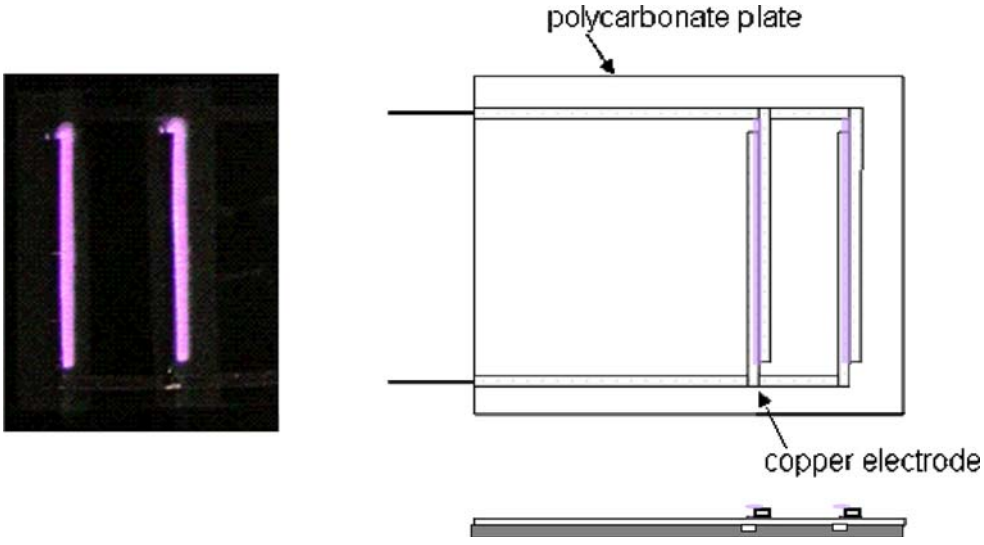

Fig. 2 Photograph (*left*) of the surface plasma generated and schematic (*right*) of a two electrode pair actuator plasma sheet

point. The response of the flow to plasma actuation was recorded photographically for qualitative interpretation of the plasma-flow interaction for Reynolds numbers as high as 3.6×10^4.

Particle image velocimetry (PIV) was used to quantitatively assess the ability of the plasma actuators to alter the flow separation and wake formation around the cylindrical body. PIV was carried out in the wake of a 5 cm diameter cylinder placed in a 30×30 cm^2 wind tunnel capable of generating air velocities up to 7.7 m/s. This smaller diameter cylinder was used in the PIV studies so that the entire wake could be captured on a single PIV image. The free stream of the tunnel was seeded with alumina (Al_2O_3) particles (nominal diameter 0.3 micron). This diameter is also sufficiently small so that electrophoretic forces on the particles can be neglected (Artana et al. 2002). The output from a double pulse Nd: YAG laser (Spectra Physics, CA, USA, PIV400) was expanded by sheet forming optics (spherical and cylindrical lenses) to illuminate the wake region of the flowfield, as shown in the schematic of Fig. 4. The two sequential laser shots (FWHM ~15 ns) separated by an adjustable time-delay generates instantaneous images of particle positions due to Mie scattering off of the particles seeded into the flow. The scattering from the particles is captured on sequential frames of a CCD camera (Kodak, ES1, Rochester, NY, USA). The particle velocities (and hence flow velocity field) are determined from differential displacement information extracted from the two images. A delay generator (DG-535, SRS) is used to vary the time delay between laser pulses and synchronize them to the camera exposure. An in-house cross-correlation code, PIVLab 2000 (see Han 2001), incorporating box offset and an iterative multi-pass procedure is used for improved vector resolution. In the PIV studies of the wake flow behind the cylinder, only two electrode pairs were used for actuation, positioned at ± 90° from the stagnation point on the cylinder. Despite the use of only two electrode pairs, a noticeable and robust control of the separation was nevertheless obtained, as described below.

We have also applied PIV to study the flow in the very near region of the electrodes. To do this, we employed a stagnation flow configuration with a single electrode pair located ~1 cm from the stagnation point. PIV images were recorded for an excitation area of up to 20×20 mm^2, immediately adjacent to the exposed electrode.

An analysis was also carried out of the optical emission from an electrode pair (ex-situ) to quantitatively evaluate the degree of thermal non-equilibrium in the plasma. This analysis was motivated by the possibility that plasma actuation of the flow may be a result of the thermal heating of the boundary layer. Measurements of the vibrational and the rotational temperature of the plasma were carried out using the intrinsic emission from the N_2 second positive system ($C^3\Pi_u$–$B^3\Pi_g$) resolved to 0.17 nm using an Ocean Optics (Model S2000) spectrometer (corrected for its relative spectral response). The vibrational and rotational temperatures were obtained by comparing the measured spectra to those computed using the Nonequilibrium Air (NEQAIR) spectral simulation program (Laux 1993). It is expected that at atmospheric pressure, the rotational and translational modes are equilibrated, and that the air temperature can be inferred from the measured rotational temperature.

3 Results

A typical current and voltage measurement for a complete AC cycle for an electrode pair is shown in Fig. 5. The discharge voltage across the electrodes is clearly out of phase with the measured current component at the same frequency (the displacement current) due to the bulk capacitance of the polycarbonate sheet. Superim-

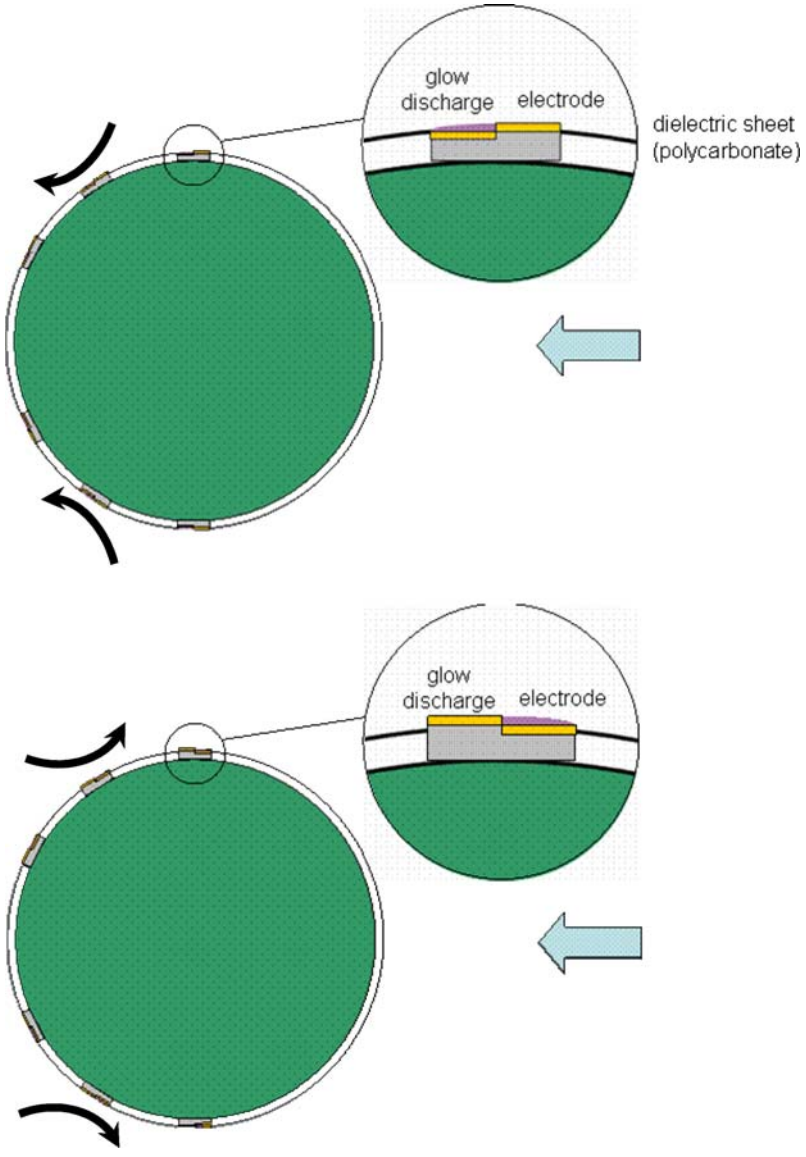

Fig. 3 Schematic illustrating the location and electrode configuration for imparting: **a** a boundary layer stabilizing force, and **b** a destabilizing force, on the downstream flow behind a cylinder

posed onto this capacitive current is the relatively large current bursts, most prominent on one swing of the AC cycle when the buried electrode is at a negative potential relative to the exposed grounded electrode. This phase of the cycle depletes the dielectric layer of its surface charge as the electrons (negative charge) stored on the dielectric surface stream toward the top electrode (Font 2004). The difference in the current bursts between the two phases of the cycle results in a higher dissipated power on the return cycle, and also an unsteady ionic wind, with a frequency that is predominantly at the driving AC frequency (Forte et al. 2005). Individual current peaks of widths of a few tens of nanoseconds superimposed onto the displacement current during this return phase are indicative of the filamentary nature of the discharge. The dissipated power (averaged over a single cycle) is estimated from the integration of the current bursts, and is typically less than ~1 W at a discharge voltage of ~5 kV, for an electrode pair that is ~5 cm in its transverse length. As seen in Fig. 6, the dissipated power increases nearly linearly with discharge voltage to ~8 kV. Beyond 8 kV, the dissipated power appears to saturate.

Typical photographs of the smoke-visualized flow around the cylinder at a condition of $Re_D = 1.8 \times 10^4$, taken from video sequences, are shown in Fig. 7. The flowfield without plasma actuation is shown in Fig. 7a. Activating the six electrode pairs, as shown in Fig. 7b, significantly alters the flowfield in the wake, due to the delay in the separation of the flow in the downstream portion of the cylinder. A close inspection of the downstream region of the cylinder shows that the plasma actuated case contains less recirculated smoke in the narrower base recirculation region. An analysis of video data indicates that there is a noticeable suppression of the Karman vortex shedding even at slightly higher Reynolds numbers $Re = 3.6 \times 10^4$, where the shift in the separation point is less apparent.

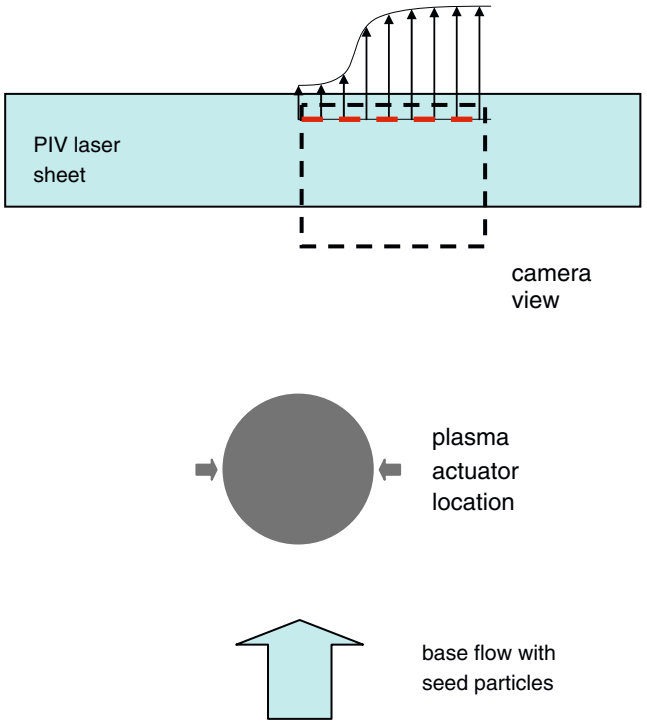

Fig. 4 Schematic of the PIV configuration for the imaging of the flow field in the wake of the cylinder

A comparison is made in Fig. 8, of the near-field flow between electrode configurations that impose a streamwise force (Fig. 8a), and electrode configurations that impose a force counter to the flow (Fig. 8b), as schematically shown in Figs. 3a,b, respectively. In the former case, the streamline visualizing the flow very near the surface appears to be fully attached, reminiscent of a wall jet, whereas in the latter case, the separation is seen to occur well into the front portion of the cylinder, at an angle of ~60° from the stagnation point. By reversing the electrode configuration, the wake (and hence drag)

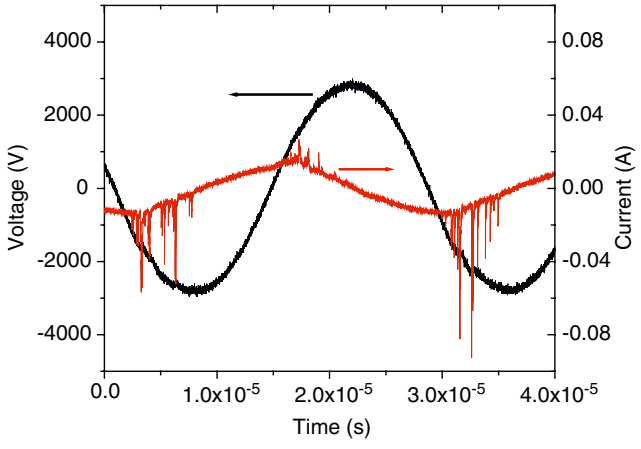

Fig. 5 Typical oscilloscope traces of the discharge voltage (buried electrode relative to grounded flow-exposed electrode) and discharge current from a single electrode pair

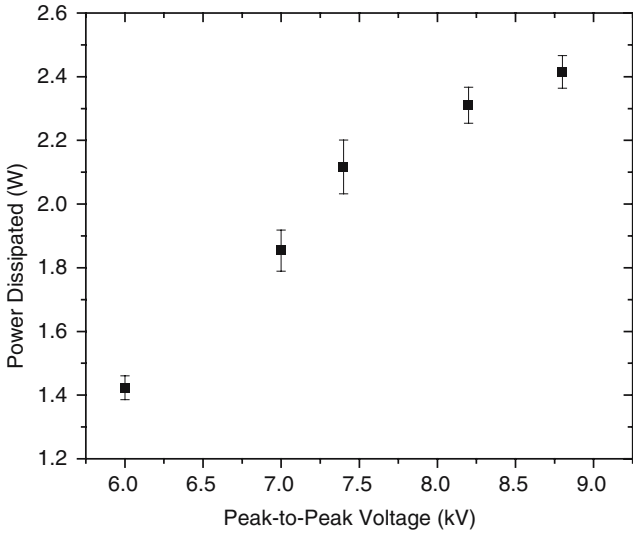

Fig. 6 Variation in the dissipated power with discharge (peak-to-peak) voltage from a single electrode pair

on the body is greatly increased. Figure 8c shows the natural case (no excitation) for comparison. This result supports the conjecture that the plasma actuation is not thermally induced—a result that is confirmed by spectroscopic studies as discussed below. We also note that the images presented here were taken from video sequences and are quite typical of the instantaneous flow.

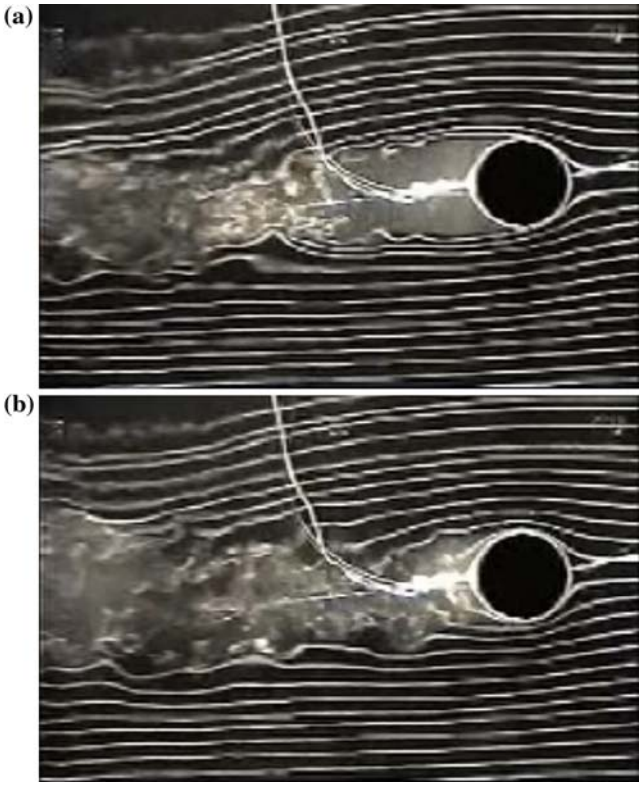

Fig. 7 Smoke visualization of plasma actuation on flow surrounding a cylinder at modest velocities (Re = 18,000): **a** plasma off, and **b** plasma on

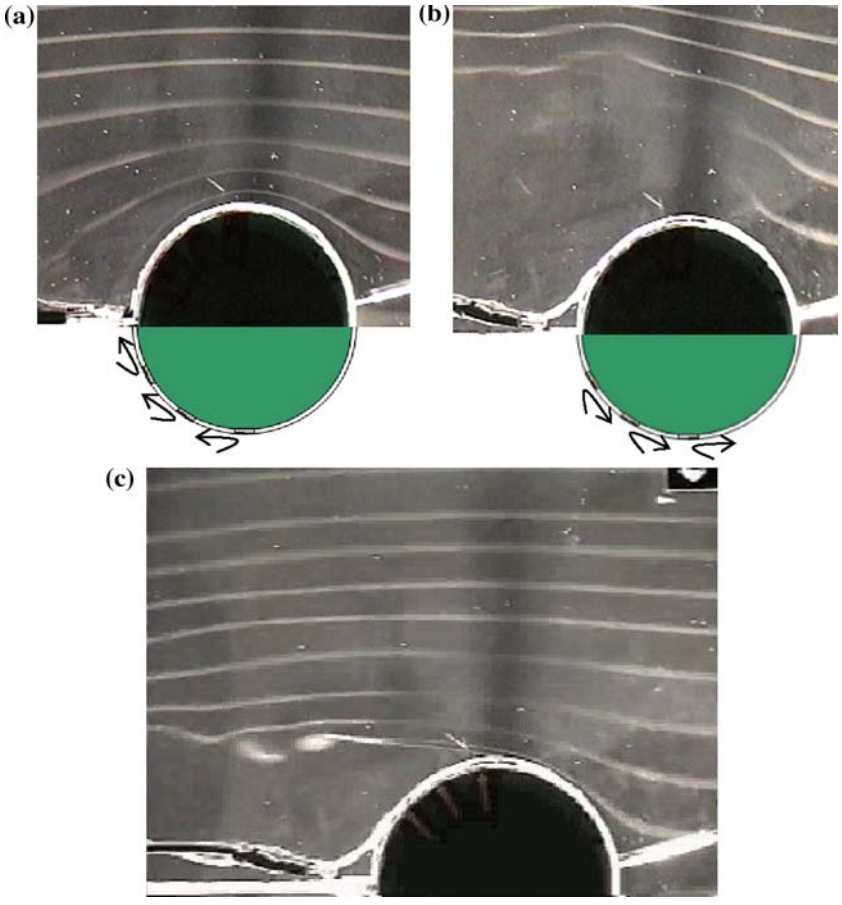

Fig. 8 Smoke visualization-schematic composites of the near field flow around the cylinders with **a** forward and **b** reversed electrode configuration (Re = 18,000). **c** Natural flow (no electrodes activated) shown for comparison. The increased wake in the reverse configuration is clearly apparent

Additionally, the flow response is essentially "instantaneous" to the naked eye when switching from actuator on to actuator off, and vice versa.

Particle Image Velocimetry was used to qualitatively visualize the velocity field and to characterize the streamwise component velocity distribution in the wake of the cylinder. Representative results obtained from an average of 150 PIV images, at a downstream position of x/D = 3 and a Re_D = 4,500 are shown in Fig. 9. In the absence of plasma excitation, the wake appears to be ~80 mm in width, with a centerline average velocity reduced to ~25% of the free stream value. There is an apparent "threshold" voltage of ~4.2–5.3 kV, below which there is little influence on the flow, even though the plasma is active. Slight increases beyond this threshold to 5.8 kV results in a dramatic narrowing of the wake (to ~40 mm in width) and a further reduction in the centerline velocity. Despite this reduction in centerline velocity, an approximate analysis of the profile confirms an overall decrease in the momentum deficit (and a reduction in drag). A further increase in voltage (to 6.7 and 7.4 kV) increases the centerline velocity without a change in the wake width and a further decrease in the momentum deficit. It should be noted that both before and after the wake has narrowed, increasing voltage leads to increasing centerline velocity (e.g., 4.2–5.3 kV and then 5.8–7.4 kV), most likely due to increasing effectiveness of the plasma actuation.

The dramatic narrowing of the wake is also seen instantaneously as illustrated by typical instantaneous PIV images of Fig. 10, which covers the range downstream of the cylinder from x/D = 2 to x/D = 3, for the same flow conditions of Fig. 9. Figure 10a is the case with the plasma off, whereas Fig. 10b is the case with the

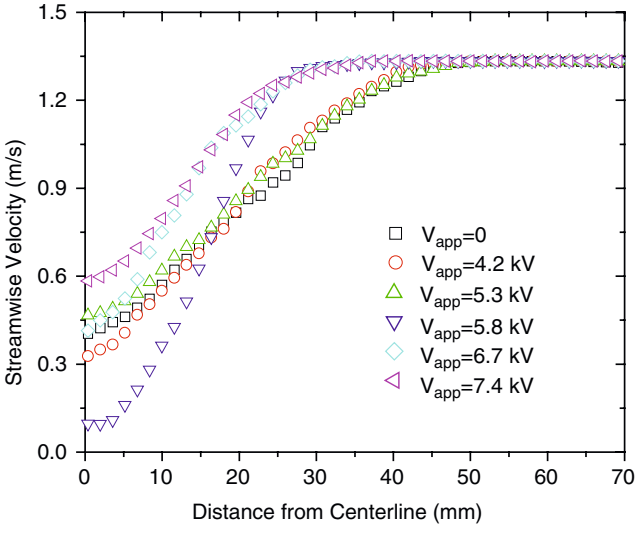

Fig. 9 Streamwise component velocity distribution in the wake of the cylinder obtained from an average of 150 PIV images, at a downstream position of x/D = 3 and a Re_D = 4,500

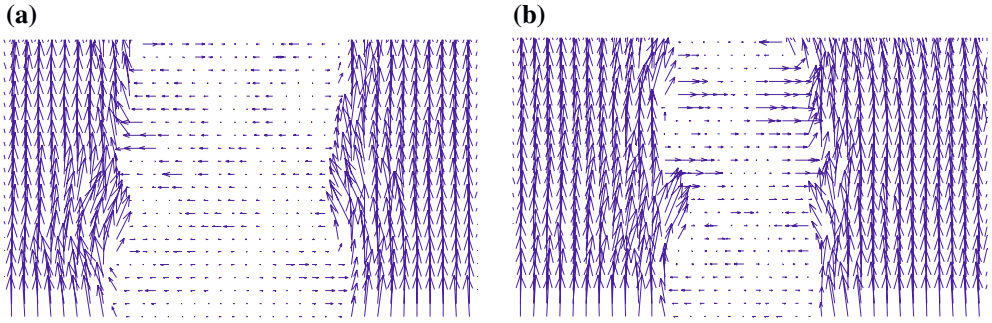

Fig. 10 Instantaneous velocity field of the cylinder wake with two electrodes mounted at 90° (x/D = 2–3, Re_D = 4,500) Freestream velocity is 1.35 m/s **a** plasma off, **b** plasma on, voltage = 5.8 kV

plasma on and the discharge voltage at 5.8 kV. Note that the time separation of the laser pulses for these PIV images is optimized to highlight the free stream flow, not the recirculating flow, thereby clearly identifying the instantaneous wake boundary.

To better understand the nature of the actuation in the near vicinity of the plasma electrodes, PIV images were taken of the flow field in an 11 × 15 mm region above a single electrode pair in a stagnation flow with a free stream velocity of 1.5 m/s, as shown in Fig. 11. The 2-mm wide electrode pair is located ~1 cm from the stagnation point in the flow. A stagnation flow configuration is chosen to demonstrate the resulting plasma-induced flow since we believe that the same phenomenon would occur locally in the vicinity of the cylinder mounted electrodes, and this configuration affords easy optical access for PIV measurements. In a representative velocity field (averaged over 60 PIV images) also shown in Fig. 11, the base flow (recorded with the plasma off) is subtracted to highlight only the effect associated with the plasma actuation. Apparent from this image is the presence of a strong "suction" toward the electrode. This finding is consistent with ionic wind velocity measurements carried out with a Pitot tube by Pons et al. (2005) who showed that the ionic wind momentum does not come from a region upstream the discharge, but a region located above the high voltage electrode, which induces suction. This suction is expected in both electrode configurations and more strongly during the return swing in the AC cycle, to satisfy mass balance due to the expected surface-parallel component of the flow in the immediate surface region–the so-called "wall jet"–that is not resolved in these PIV images. Figure 11 also shows an apparent suction effect downstream of the actuator which might seem unexpected; however, since a wall jet is produced downstream of the actuator, the entrainment of fluid by the jet as it develops along the wall is consistent with the downstream suction seen here. As was the case for the cylinder flow studies, we found that in these stagnation point flow studies, there is a voltage "threshold", before which the plasma has little effect on the flow. At a voltage of 4.2 kV, though the plasma is excited (discharge is on), the flow field is found to be unaffected by the presence of the plasma. For the case shown in the figure, the threshold voltage was identified to be ~5.8 kV. Beyond this limit, our studies indicate that the strength of the "suction" increases with increased voltage. Artana et al. (2002) have shown that for an electric field of $\sim 10^6$ V/m and typical PIV seed particles of ~0.3 μm diameter as used here, the influence of Coulombian forces on the flow tracers can be neglected. We do note however, that electrophoretic forces will likely exist on the seed particles in the very highest electric field region very close to the electrodes, and these have not been accounted for, so some caution is needed in interpreting Fig. 11 owing to the added uncertainty.

The filamentary DBD spectrum in air contains strong emission from the N_2 second positive system ($C^3\Pi_u$–$B^3\Pi_g$) as shown in Fig. 12. Also shown in Fig. 12 is a superimposed simulated spectrum using the NEQAIR

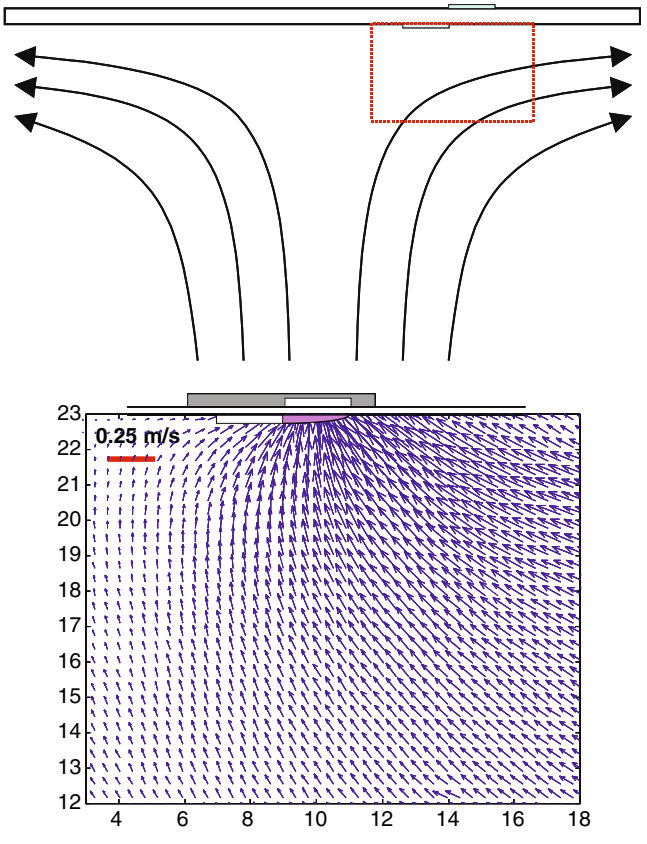

Fig. 11 The PIV-generated velocity field in the vicinity of an electrode in a stagnation flow configuration (*top*). The PIV data (*bottom panel*) is a 60-shot average with the undisturbed base flow subtracted, clearly illustrating the "suction" like actuation. Field of view is show in mm

code, with the vibrational and rotational temperature used as a fitting parameter. The vibrational temperature is primarily determined by the intensity ratios of the vibrational bands while the rotational temperature is determined by the shape (rotational structure) of individual vibrational bands. For the spectrum in Fig. 12, the best fit results in T_{rot} = 285 K and T_{vib} = 3,165 K, with estimated uncertainties of 20 and 5%, respectively. The low rotational temperature further confirms the non-equilibrium nature of the discharge, and the likeliness that the actuation is not a result of a thermal process due to ohmic heating of the boundary layer.

4 Summary

These results demonstrate that modest discharge power invested by a dielectric barrier discharge into the boundary layer significantly reduces wake momentum deficit by influencing flow separation of a bluff body. We further demonstrate that an opposite electrode configuration can be used to effect greater separation as opposed to improved reattachment; such a configuration could be advantageous in enhancing mixing or flow vectoring. PIV was used to quantify changes in the wake structure, in particular, the narrowing of the wake at high discharge voltages. The PIV was also able to reveal the presence of a suction effect close to the electrodes in a stagnation flow configuration. The suction phenomenon is expected in either electrode configuration (even when the plasma acts to impart a force against the flow), and is not believed to be the only mechanism for boundary layer stabilization. Numerical simulations (Font 2004) suggest that the stabilization is also expected to be from an unresolved "wall jet", developed by the ion drag during the surface discharging swing in the AC cycle, also seen experimentally by Forte et al. (2005). Finally, spectral measurements and simulations accounting for vibrational-rotational non-equilibrium suggest that the plasma effect is not a thermal effect, being attributed instead to the non-equilibrium nature of the discharge resulting in low rotational and high vibrational temperatures. While these results have been demonstrated for moderate Reynolds numbers, future work aimed at higher Reynolds numbers and investigations of the wall jet appear warranted.

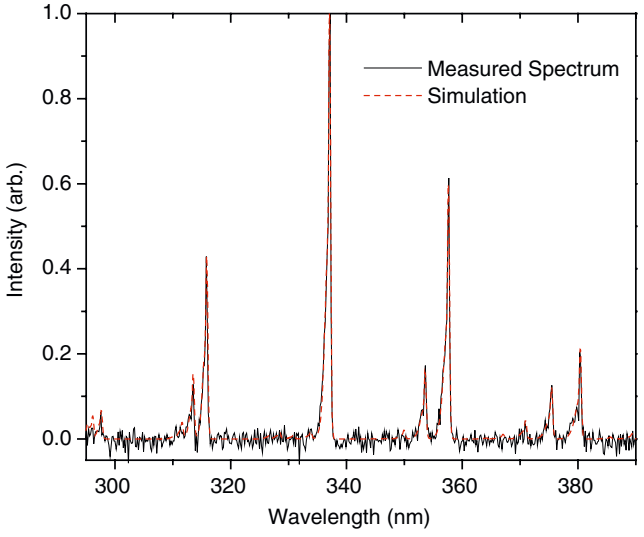

Fig. 12 Measured (*solid*) and predicted (*dashed*) N_2 second positive spectrum from the discharge-excited air. To obtain such a good fit to the measured spectrum, it was necessary to assume T_{rot} = 285 K and T_{vib} = 3,165 K

Acknowledgments This work was supported in part through a Stanford University–Seoul National University student exchange program in 2001–2002. The research conducted by Y. Sung was published as his M.S. dissertation at SNU in August 2002.

References

Artana G, D'Adamo J, Leger L, Moreau E, Touchard G (2002) Flow control with electrohydrodynamic actuators. AIAA J 9:1773–1779

Artana G, Sosa R, Moreau E, Touchard G (2003) Control of the near-wake flow around a circular cylinder with electrohydrodynamic actuators. Exp Fluids 35:580–588

Enloe CL, McLaughlin TE, Van Dyken RD, Kachner KD, Jumper EJ, Corke TC, Post M, Haddad O (2004a) Mechanisms and responses of a single dielectric barrier plasma actuator: geometric effects. AIAA J 42:595–604

Enloe CL, McLaughlin TE, Van Dyken RD, Kachner KD (2004b) Mechanisms and response of a single dielectric barrier plasma actuator: plasma morphology. AIAA J 42:589–594

El-Khabiry S, Colver GM (1997) Drag reduction by dc corona discharge along an electrically conductive flat plate for small Reynolds number flow. Phys Fluids 9:587–599

Forte M, Léger L, Pons J, Moreau E, Touchard G (2005) Plasma actuators for airflow control: measurement of the non-stationary induced flow velocity. J Electrostatic 63:929–936

Font GI (2004) Boundary layer control with atmospheric plasma discharges AIAA paper 2004–3574

Han D (2001) Study of nonpremixed jet flames using simultaneous measurements of velocity and CH distribution. Ph.D Thesis, Stanford University, Stanford

Hyun KT, Chun CH (2003) The wake flow control behind a circular cylinder using ion wind. Exp Fluids 35:541–552

Kogelschatz U, Eliasson B, Egil W (1997) Fundamentals and applications of dielectric barrier discharges. In: proceedings of the 23rd ICPIG, pp1–20

Laux CO (1993) Optical diagnostics and radiative emission of air plasmas. Ph. D Thesis, Stanford University, Stanford

Malik MR, Weinstein LM, Hussani MY (1983) Ion wind drag reduction. AIAA Paper 83–0231

Pons J, Moreau E, Touchard G (2005) Asymmetric surface dielectric barrier discharge in air at atmospheric pressure: electrical properties and induced airflow characteristics. J Phys D Appl Phys 38:3635–3642

Post ML, Corke TC (2004) Separation control on a high angle of attack airfoil using plasma actuators. AIAA J 42:2177–2184

Roth JR (2003) Aerodynamic flow acceleration using paraelectric and peristaltic electrohydrodynamic effect of a one atmosphere uniform glow discharge plasma. Phys Plasmas 10:2117–2126

Roth JR, Sherman DM (1998) Boundary layer flow control with a one atmosphere uniform glow discharge surface plasma. AIAA Paper 98–0328

Roth JR, Sherman DM, Wilkinson SP (2000) Electrohydrodynamic flow control with a glow-discharge surface plasma. AIAA J 38:1166–1172